Diffraction: Real Samples
Powder Method

Diffraction: Real Samples

- Up to this point we have been considering diffraction arising from infinitely large crystals that are strain free and behave like ideally imperfect materials (x-rays only scattered once within a crystal)
- Crystal size and strain affect the diffraction pattern
  - we can learn about them from the diffraction pattern
- High quality crystals such as those produced for the semiconductor industry are not ideally imperfect
  - need a different theory to understand how they scatter x-rays
- Not all materials are well ordered crystals

Crystallite Size

- As the crystallites in a powder get smaller the diffraction peaks in a powder pattern get wider.
- Consider diffraction from a crystal of thickness t and how the diffracted intensity varies as we move away from the exact Bragg angle
  - If thickness was infinite we would only see diffraction at the Bragg angle

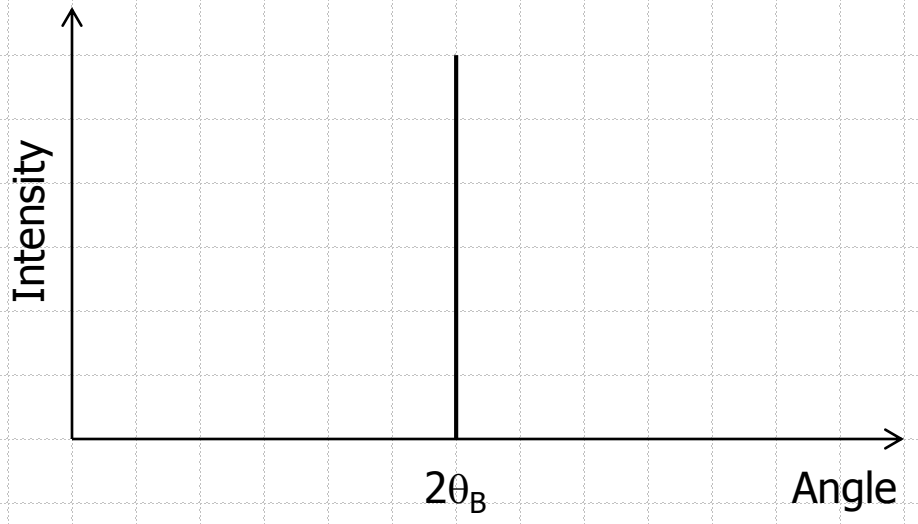

Crystallite Size

Suppose the crystal of thickness t has $(m + 1)$ planes in the diffraction direction.
Let say θ is variable with value θ_B that exactly satisfies Bragg's Law:

$$\lambda = 2d \sin \theta_B$$

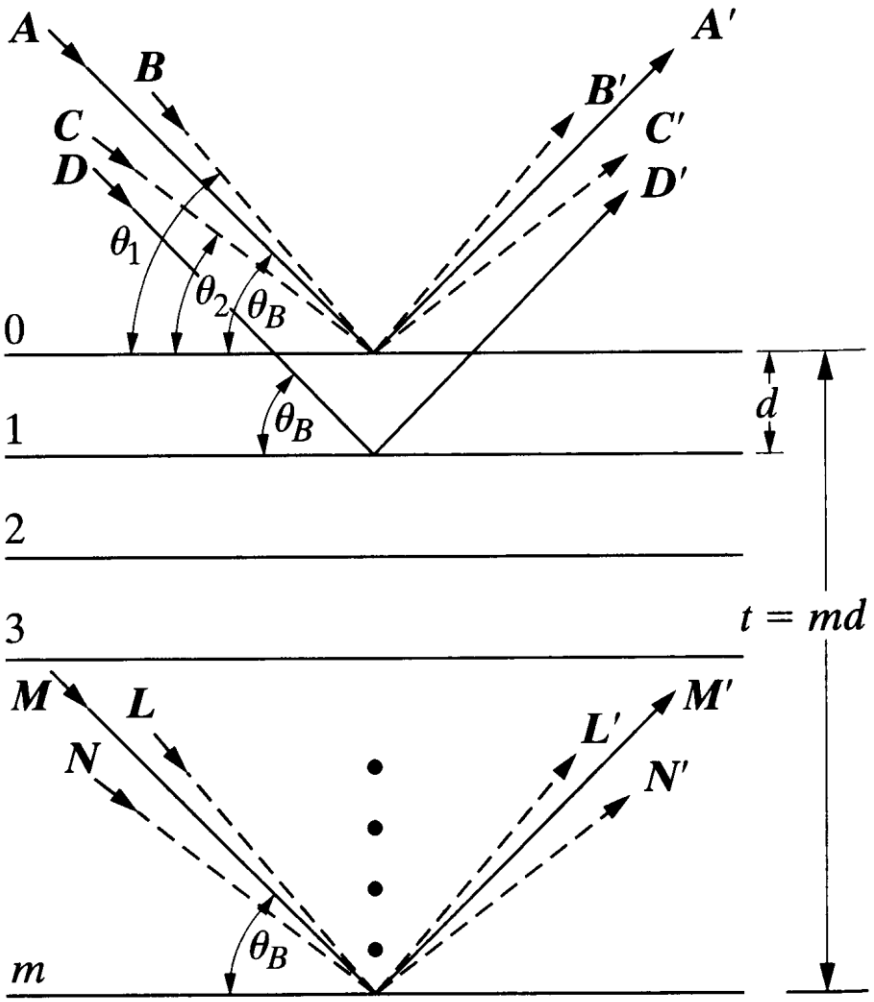

- Rays **A**, **D**, …, **M** makes angle θ_B
- Rays **B**, …, **L** makes angle θ_1
- Rays **C**, …, **N** makes angle θ_2

Crystallite Size

- For angle θ_B diffracted intensity is maximum
- For θ_1 and θ_2 – intensity is 0.
- For angles $\theta_1 > \theta > \theta_2$ – intensity is nonzero.

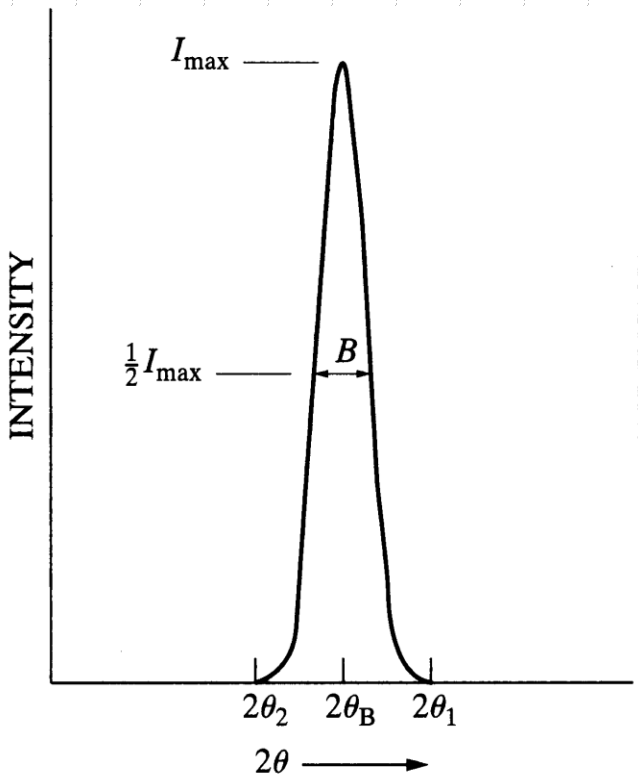

Real case

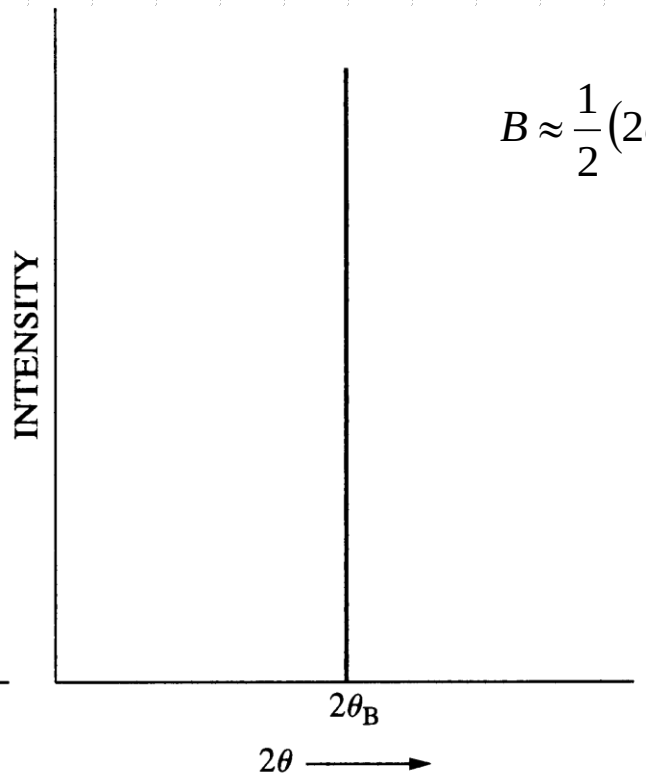

Ideal case

$$B \approx \frac{1}{2}(2\theta_1 - 2\theta_2) = \theta_1 - \theta_2$$

The Scherrer Equation

$$2t\sin\theta_1 = (m+1)\lambda,$$
$$2t\sin\theta_2 = (m-1)\lambda.$$

Subtracting:

$$t(\sin\theta_1 - \sin\theta_2) = \lambda,$$
$$2t\cos\left(\frac{\theta_1+\theta_2}{2}\right)\sin\left(\frac{\theta_1-\theta_2}{2}\right) = \lambda.$$

θ_1 and θ_2 are close to θ_B, so:

$$\theta_1 + \theta_2 \approx 2\theta_B,$$
$$\sin\left(\frac{\theta_1-\theta_2}{2}\right) \approx \left(\frac{\theta_1-\theta_2}{2}\right).$$

Thus:

$$2t\left(\frac{\theta_1-\theta_2}{2}\right)\cos\theta_B = \lambda,$$
$$t = \frac{\lambda}{B\cos\theta_B}$$

The Scherrer Equation

Instrument broadening has to be subtracted

- More exact treatment (see *Warren*) gives:

$$t = \frac{0.94\lambda}{B\cos\theta_B}$$ ← Scherrer's formula

- Peak width *B* varies inversely with the crystallite size.
- The proportionality constant, *K*, is usually 0.94 and is valid for spherical crystals with cubic symmetry when *B* is taken as full width at half maximum (FWHM).
- The proportionality constant, *K*, is 0.89 for spherical crystals with cubic symmetry when *B* is taken as integral breadth.
- *K* sometimes is rounded up to 1.
- *K* might vary from 0.62 to 2.08.

Suppose λ = 1.54 Å, *d* = 1.0 Å, and θ = 49°:

for crystal size of 1 mm, *B* = 10^{-5} deg.
for crystal size of 500 Å, *B* = 0.2 deg.

Peak Width

- Full Width at Half Maximum (FWHM):
  - Width of the peak at half intensity value between background and peak maximum intensity.

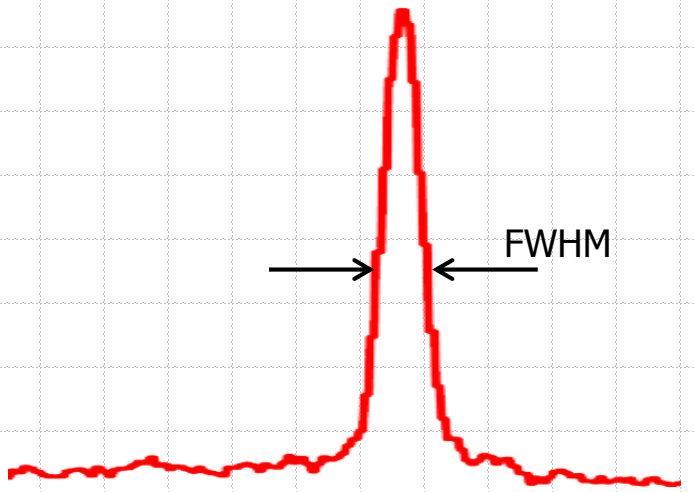

- Integral Breadth:
  - Total area under the peak divided by the peak height.
  - Same as the width of a rectangle which has the same area and the same height as the peak

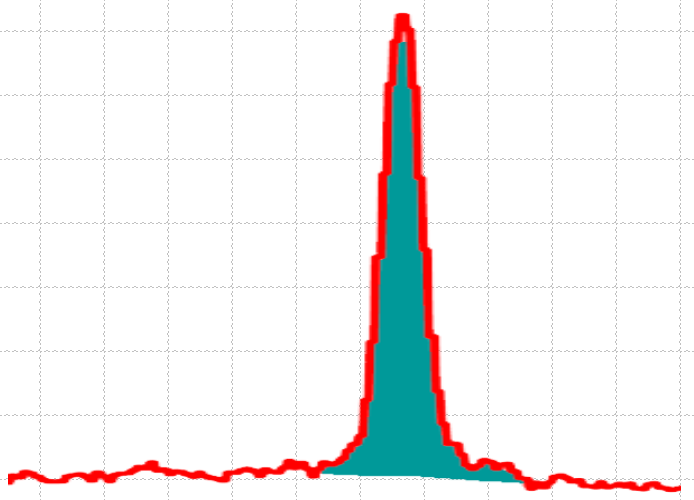

Williamson-Hall Plot

Instrument broadening has to be subtracted

- Size broadening (Scherrer equation): $B_t(2\theta) = \frac{K\lambda}{t\ cos\theta}$
- Strain broadening: $B_\varepsilon(2\theta) = 4\varepsilon\ tan\theta$
- Convoluted broadening: $B_{tot}(2\theta) = B_t(2\theta) + B_\varepsilon(2\theta) = \frac{K\lambda}{t\ cos\theta} + 4\varepsilon\ tan\theta$

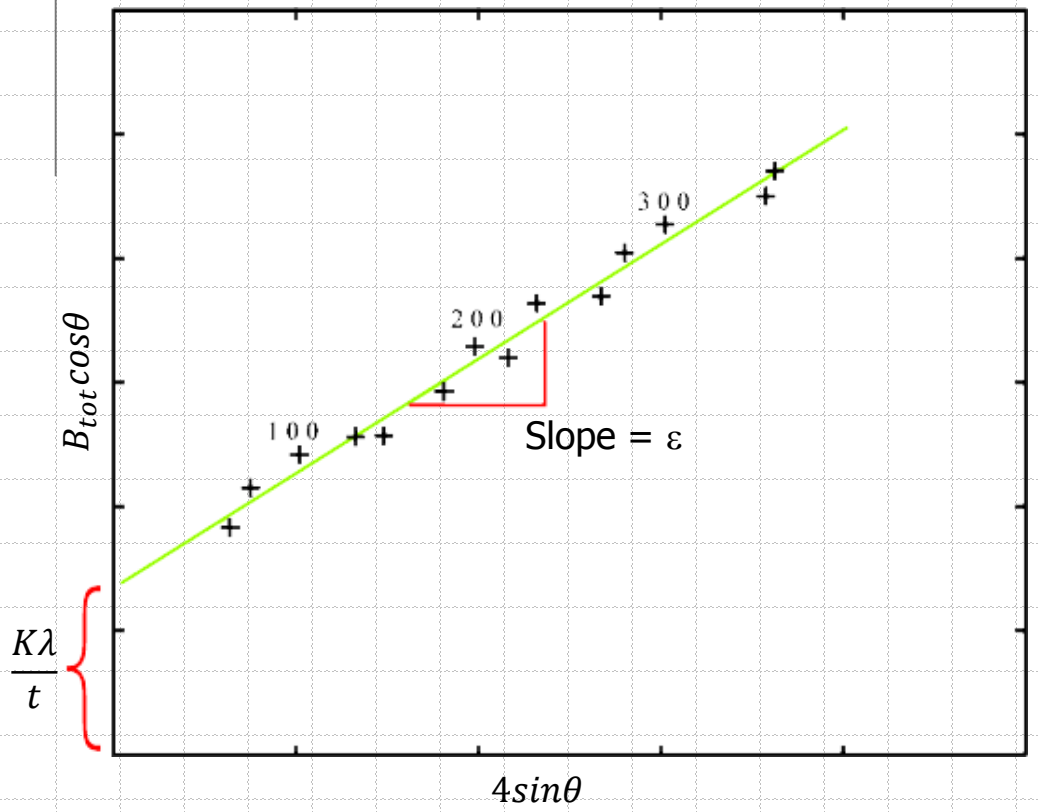

$$B_{tot}cos\theta = \frac{K\lambda}{t} + 4\varepsilon\ sin\theta$$

Corrections for Instrumental Broadening

- There is a link between peak width and crystallite size/strain, but other sources of peak broadening have to be considered when analyzing diffraction data
  - Instrumental broadening:
    - slit widths
    - sample size
    - penetration in the sample
    - imperfect focusing
    - unresolved α_1 and α_2 peaks
    - or wavelengths widths where α_1 and α_2 peaks are resolved

- To correct for instrumental broadening:
  - measure the sample
  - measure under the same conditions the standard with unstrained particles large enough to eliminate particle-size broadening

Corrections for Instrumental Broadening

- Lorentzian shape:

$$B_{obs} = B_{size} + B_{strain} + B_{inst}$$

$$(B_{obs} - B_{inst}) = B_{size} + B_{strain}$$

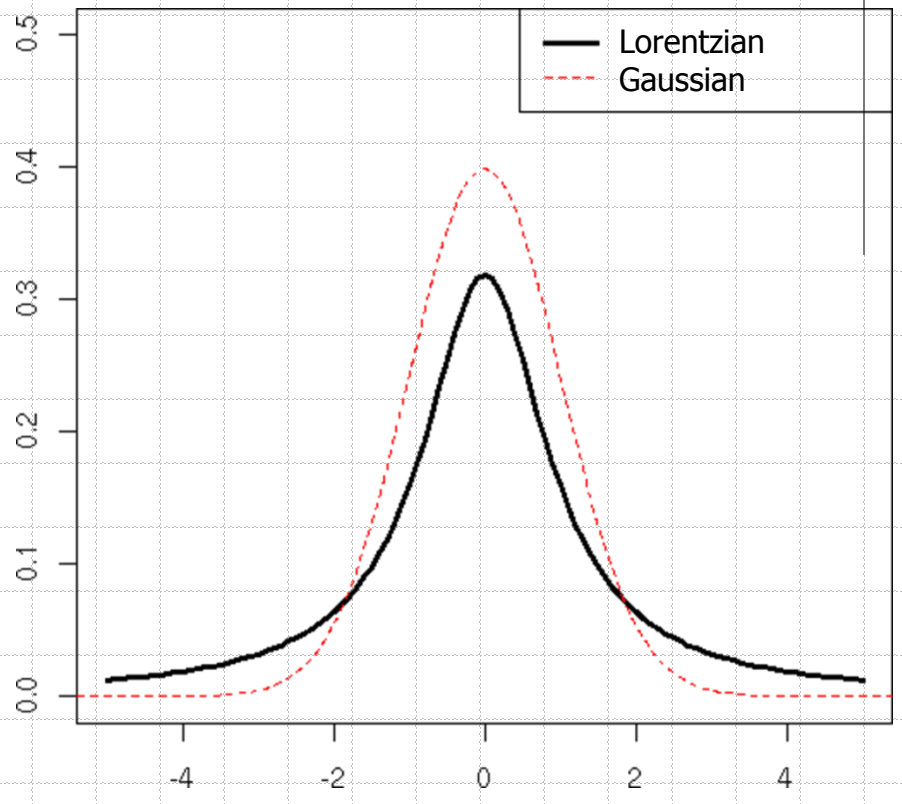

- Gaussian shape:

$$B_{obs}^2 = B_{size}^2 + B_{strain}^2 + B_{inst}^2$$

$$\left(B_{obs}^2 - B_{inst}^2\right) = B_{size}^2 + B_{strain}^2$$

- Voigt, Pseudo-Voigt:
  - Deconvolute peaks into gaussian and lorentzian fractions and then subtract instrumental broadening.

Interference Function

- We calculate the diffraction peak at the exact Bragg angle θ_B and at angles that have small deviations from θ_B.
- If crystal is infinite then at $\theta \neq \theta_B$ intensity = 0.
- If crystal is small then at $\theta \neq \theta_B$ intensity $\neq$ 0. It varies with angle as a function of the number of unit cells along the diffraction vector ($\mathbf{s} - \mathbf{s}_0$).
- At deviations from θ_B individual unit cells will scatter slightly out of phase.
- Vector ($\mathbf{s} - \mathbf{s}_0$)/$\lambda$ no longer extends to the reciprocal lattice point (RLP).

$$\frac{(\mathbf{s}-\mathbf{s_0})}{\lambda} = h\mathbf{b_1} + k\mathbf{b_2} + l\mathbf{b_3}$$

Interference Function

- $\theta(1) > \theta_B(1)$ for 001 and $\theta(2) > \theta_B(2)$ for 002
- If $\mathbf{H}_{hkl} = \mathbf{H}$ is reciprocal lattice vector then $(\mathbf{s} - \mathbf{s}_0)/\lambda \neq \mathbf{H}$.

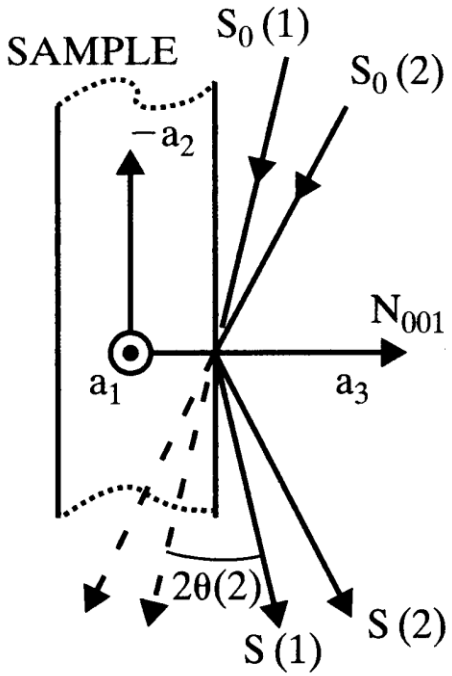

Real space

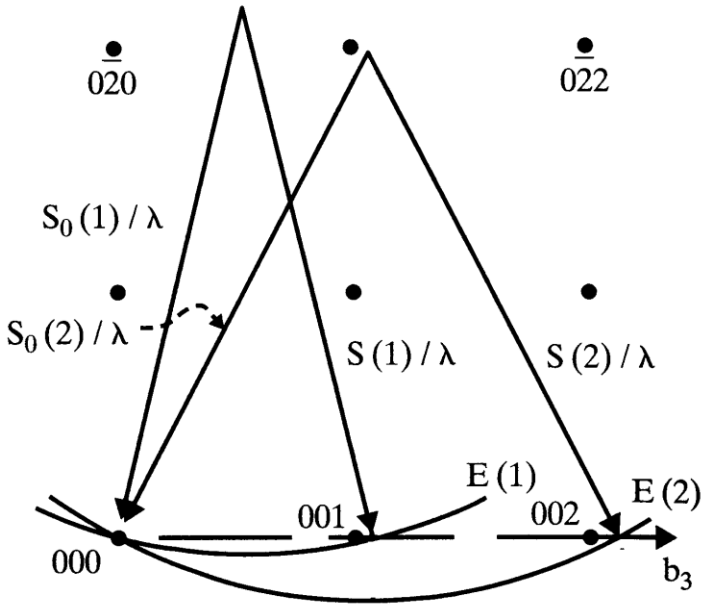

Reciprocal space

Interference Function

- We define:

$$\left(\mathbf{S}-\mathbf{S_0}\right)/\lambda-\mathbf{H}=\ell$$

as deviation parameter

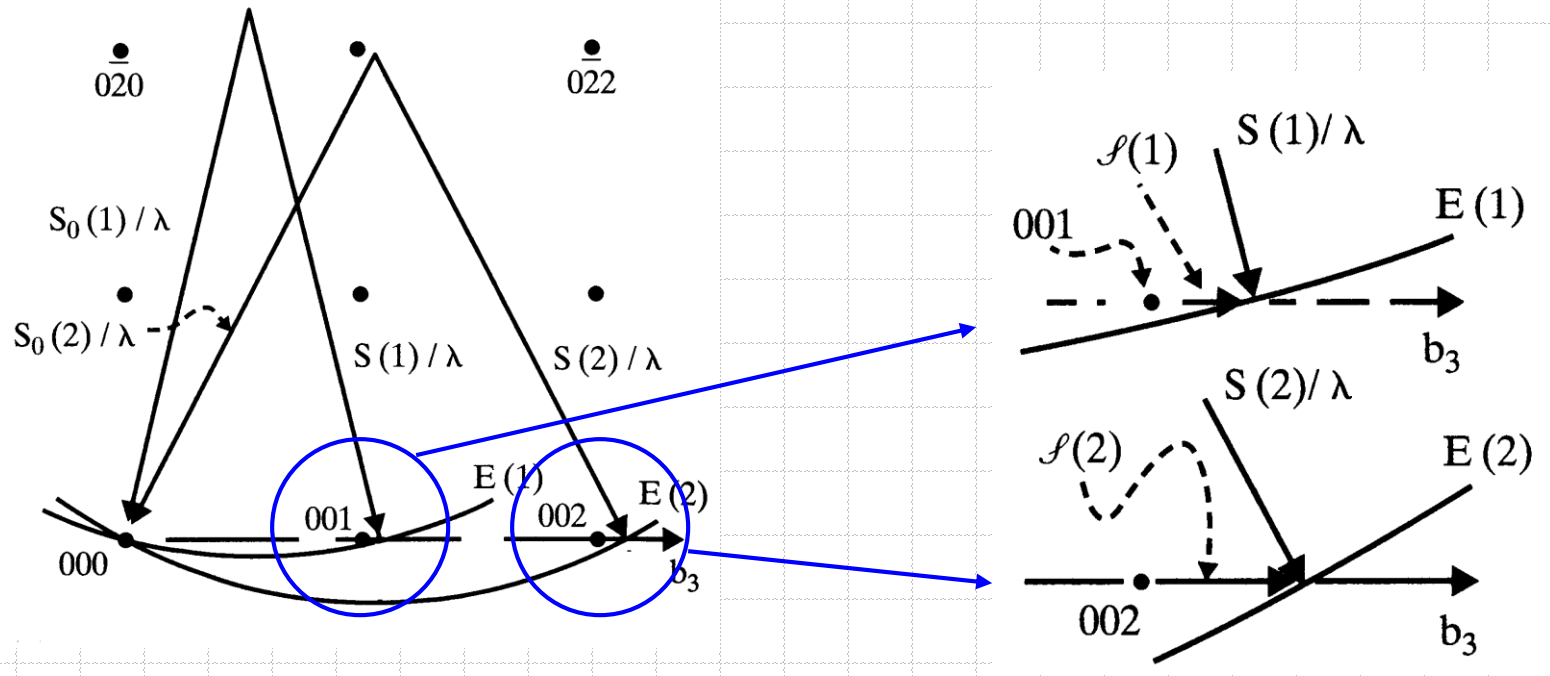

Interference Function

- In order to calculate the intensity diffracted from the crystal at $\theta \neq \theta_B$, the phase differences from different unit cells must be included.
- For three unit vectors $\mathbf{a}_1$, $\mathbf{a}_2$ and $\mathbf{a}_3$:

$$A_{total} = \sum_{n_1=0}^{N_1-1} \sum_{n_2=0}^{N_2-1} \sum_{n_3=0}^{N_3-1} F \exp \frac{2\pi i}{\lambda} \left[\left(\mathbf{s} - \mathbf{s_0} \right) \cdot \left(n_1 \mathbf{a}_1 + n_2 \mathbf{a}_2 + n_3 \mathbf{a}_3 \right) \right]$$

n_i – particular unit cell
N_i – total number of unit cells along $\mathbf{a}_i$

From the definition of the reciprocal lattice vector:

$$\left(\mathbf{s} - \mathbf{s_0} \right) / \lambda = \mathbf{H} + \ell = \left(h_1 \mathbf{b}_1 + k_2 \mathbf{b}_2 + l_3 \mathbf{b}_3 \right) + \ell$$

Interference Function

$$A_{total} = F\sum_{n_1}\sum_{n_2}\sum_{n_3}\exp\left[2\pi i\left(\mathbf{H}+\ell\right)\cdot\left(n_1\mathbf{a}_1+n_2\mathbf{a}_2+n_3\mathbf{a}_3\right)\right]$$

$$= F\sum_{n_1}\sum_{n_2}\sum_{n_3}\exp\left[2\pi i\left(h_1\mathbf{b}_1+k_2\mathbf{b}_2+l_3\mathbf{b}_3+\ell\right)\cdot\left(n_1\mathbf{a}_1+n_2\mathbf{a}_2+n_3\mathbf{a}_3\right)\right]$$

since: $\mathbf{b}_j\cdot\mathbf{a}_i=\delta_{ij}$

$$A_{total} = F\sum_{n_1}\exp\left(2\pi i\ell\cdot n_1a_1\right)\sum_{n_2}\exp\left(2\pi i\ell\cdot n_2a_2\right)\sum_{n_3}\exp\left(2\pi i\ell\cdot n_3a_3\right)$$

Converting from exp to sines:

$$A_{total} = F\left[\prod_{i=1}^{3}\frac{\sin\pi\lambda\ell\cdot N_i\mathbf{a}_i}{\sin\pi\lambda\ell\cdot\mathbf{a}_i}\right]\exp\left\{\pi\left[\left(N_1-1\right)\mathbf{a}_1+\left(N_2-1\right)\mathbf{a}_2+\left(N_3-1\right)\mathbf{a}_3\right]\right\}$$

Interference Function

- Calculating intensity we lose phase information therefore:

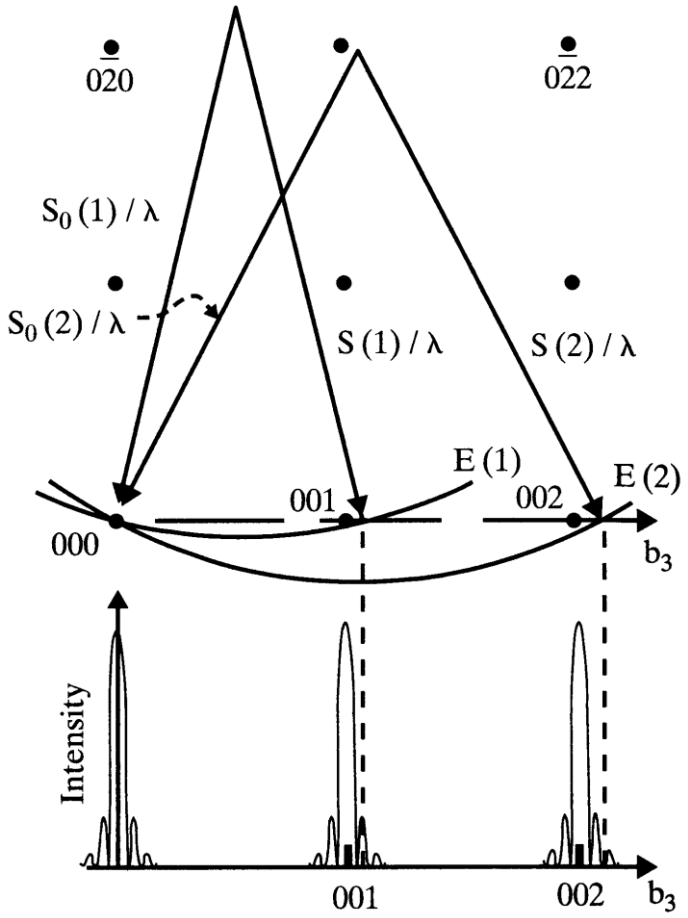

$$I = \left| A_{total} \right|^2$$

$$I = F^2 \prod_{i=1}^{3} \frac{\sin^2 \pi\lambda\ell \cdot N_i \mathbf{a}_i}{\sin^2 \pi\lambda\ell \cdot \mathbf{a}_i}$$

interference function

Maximum intensity at Bragg peak is F^2N^2
Width of the Bragg peak $\propto$ 1/N

N is a number of unit cells along (**s** - $\mathbf{s_0}$)

Interference Function

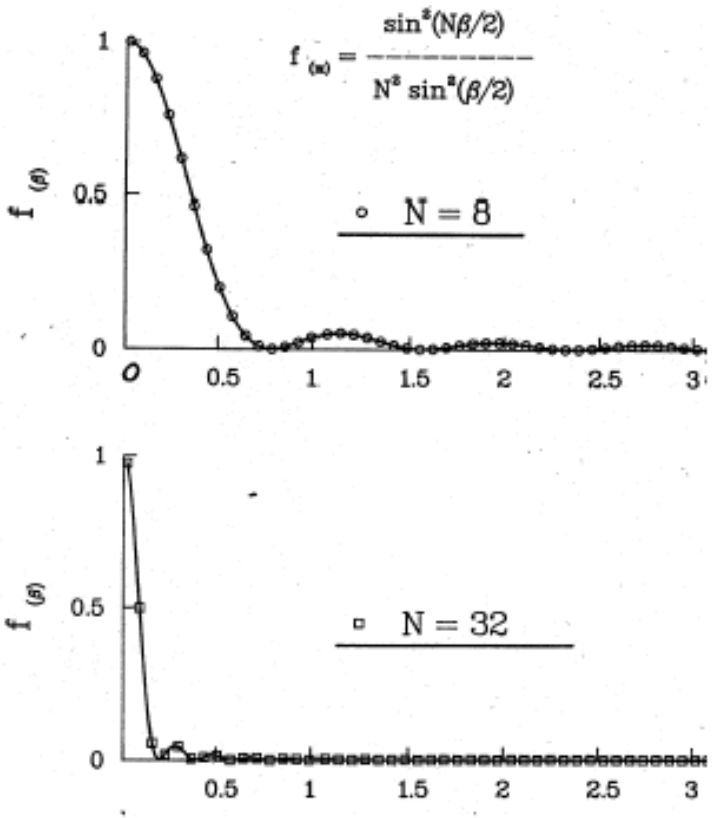

For reasonable number of unit cells, ripples beyond main peak are very weak

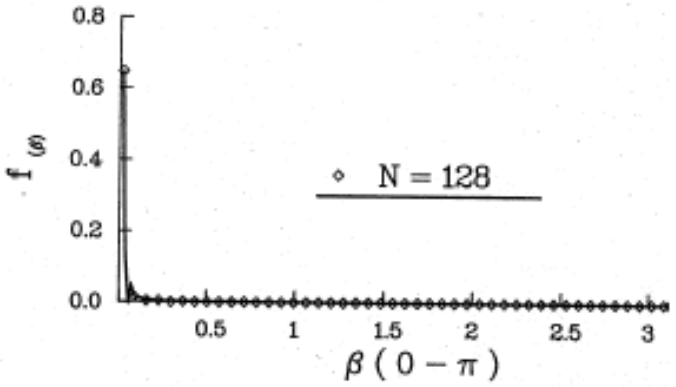

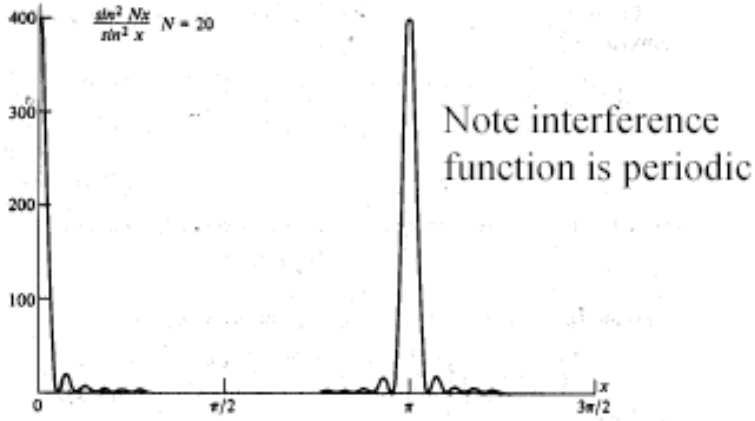

Fig. 3.2 The function $(\sin^2 Nx)/\sin^2 x$ for $N = 20$. The function peaks at values of x which are integral multiples of π, and it is essentially zero everywhere else.

Crystallite Size

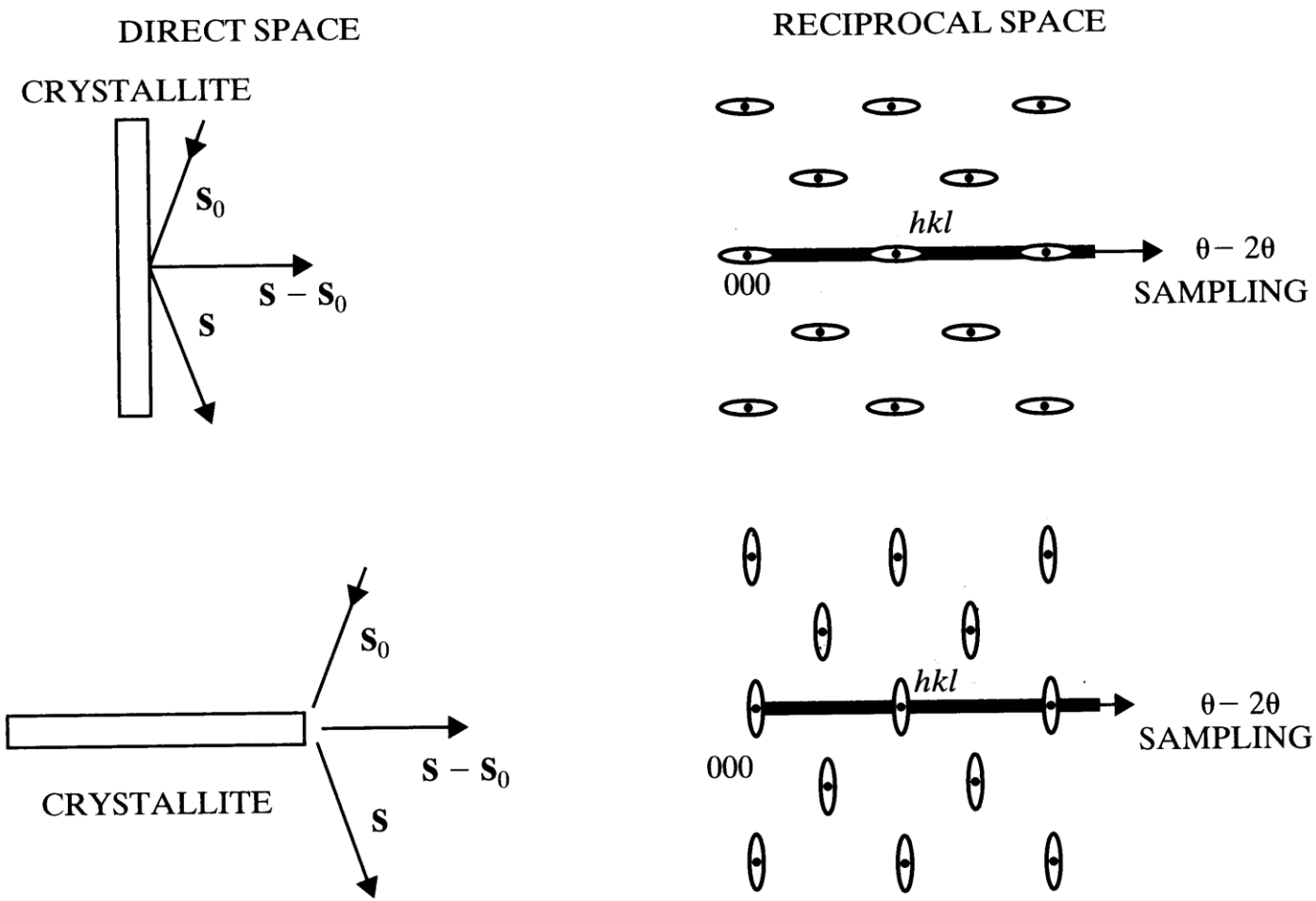

Perfect Crystals

- The diffracted intensity calculations make use of ideally imperfect crystals
- This is the "kinematical" theory of diffraction
- The integrated intensity from a perfect crystal – large and no mosaic blocks – is less than that from an ideally imperfect crystal
- Our consideration of Bragg peak width also has some problems. When we have very large perfect crystals the peak width is not zero. The width converges to a finite small value as the size of the crystal increases
- We need a better theory!
- Dynamical theory is used to treat diffraction in perfect crystals

Perfect Crystals

- Dynamical diffraction theory is complicated. It includes the possibility of multiple scattering in a crystal. Diffracted beam is phase shifted by 90° every time it is diffracted within the crystal (this is in addition to the 180° shift on scattering from an individual electron or atom)
  - Scattering twice off a set of lattice planes K_0 to K_1 to K_2, produces a diffracted beam in the direction of the incident beam but with a 180° phase shift. The resulting destructive interferences reduces the intensity of the beam in the incident direction
  - This is PRIMARY EXTINCTION

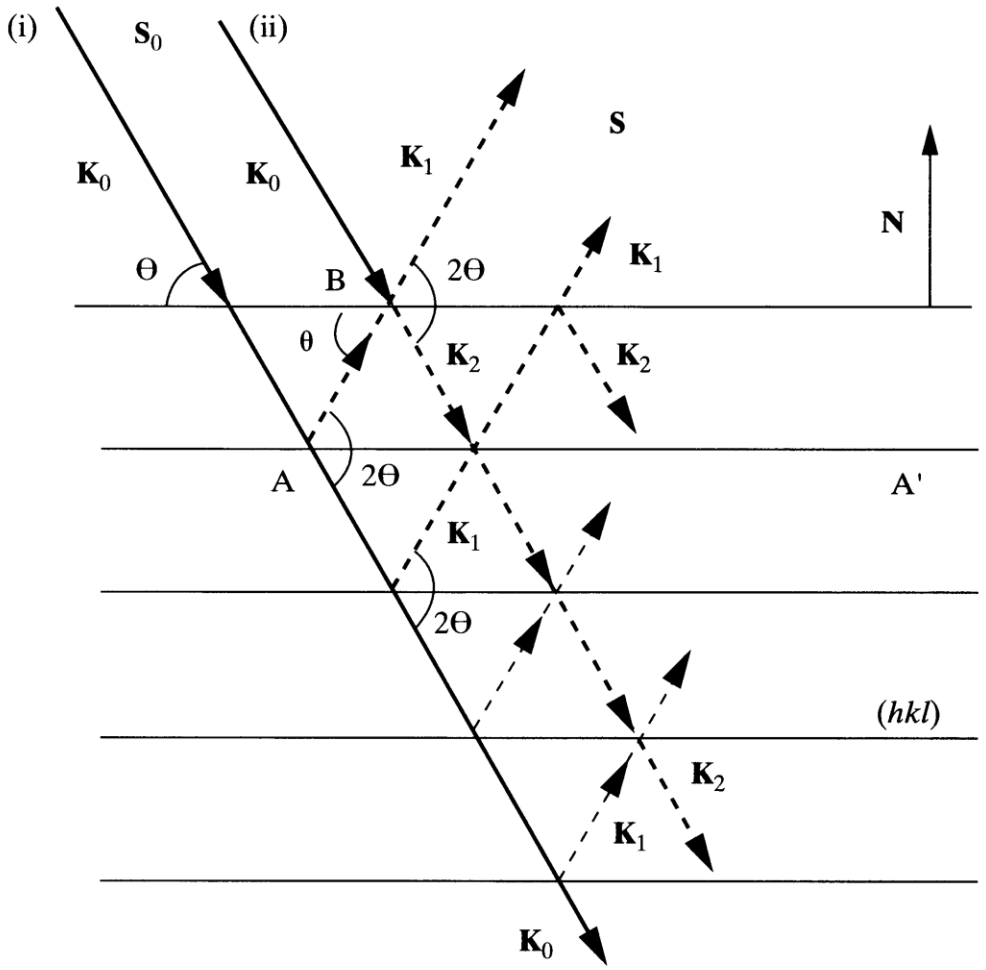

Perfect Crystals

- A full mathematical treatment of dynamical theory uses differential equations that describe the transfer of energy between the forward and diffracted x-ray beams.

- This theory predicts that intensity from a perfect crystal with negligible absorption is

$$I = \frac{8}{3\pi}\left(\frac{e^2}{mc^2}\right)\frac{N\lambda^2|F|}{\sin 2\theta}\left(\frac{1+|\cos 2\theta|}{2}\right)$$

where N is the number of unit cells per unit volume.

Note the intensity depends on F not F^2

Perfect Crystals

- The theory also predicts that the peak shape on rocking the crystal in the diffracted beam. The width of this rocking curve is called the Darwin width. Note that at the top of the curve the reflectivity is ~100%.

- The width of the curve 2s is given by

$$s = \left(\frac{e^2}{mc^2}\right)\frac{N\lambda^2|F|}{\pi \sin 2\theta}\left(\frac{1+|\cos 2\theta|}{2}\right)$$

FWHM, $\Delta\theta_0$, for Darwin curve = $2.12s$

For first order reflections:
5 arcs < $\Delta\theta_0$ < 20 arcs

Higher order reflections have considerably narrower rocking curves

Changes in shape: due to absorption

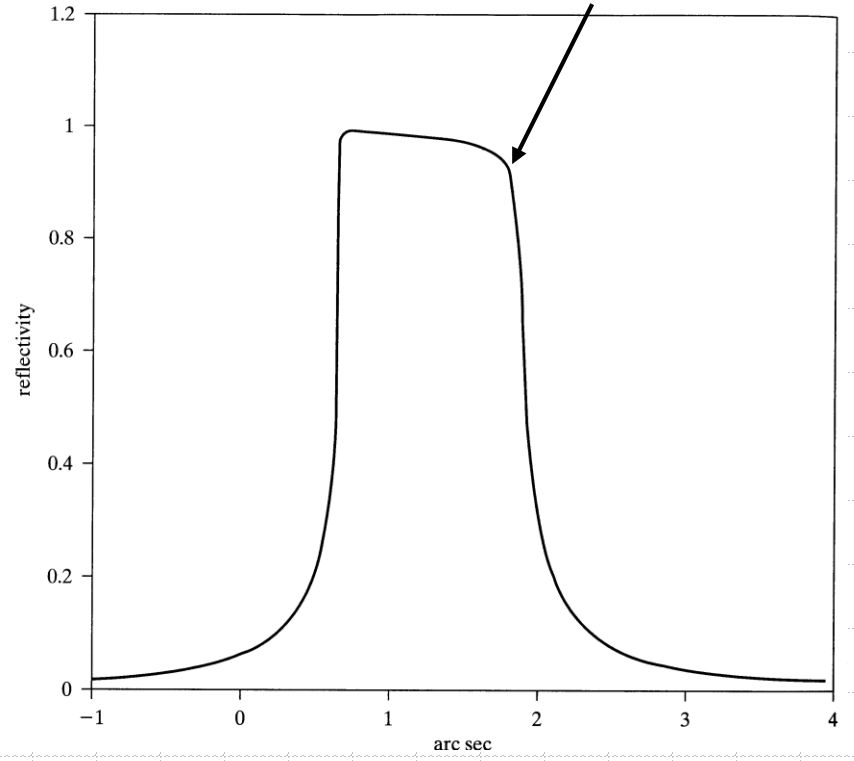

The Powder Diffraction File

- Experience has shown that the ensemble of *d*-spacings ("*d*" s) and intensities ("*I*" s) is sufficiently distinctive in order to identify phases
- Phase determination can be performed by a comparison of a set of experimental *d*'s and *I*'s with a database of *d*-*I* files
- *d* - spacings are independent of wavelength
- Intensities are relative (most intense = 100 or 1000 or 1)

Powder Diffraction File (PDF) Database

- 1919 -- Hull pointed out that powder diffraction could be used for routine chemical analyses
  - powder pattern is characteristic of the substance
  - the patterns of a combination of phases will superimpose
  - only a small amount is needed
- 1938 -- Hanawalt, Rinn and Frevel at Dow Chemical compiled diffraction data on about 1000 compounds as 3”x5” file cards and devised a simple means of classifying the data
- 1942 -- the American Society for Testing Materials (ASTM) published the first edition of diffraction data cards (1300 entries)

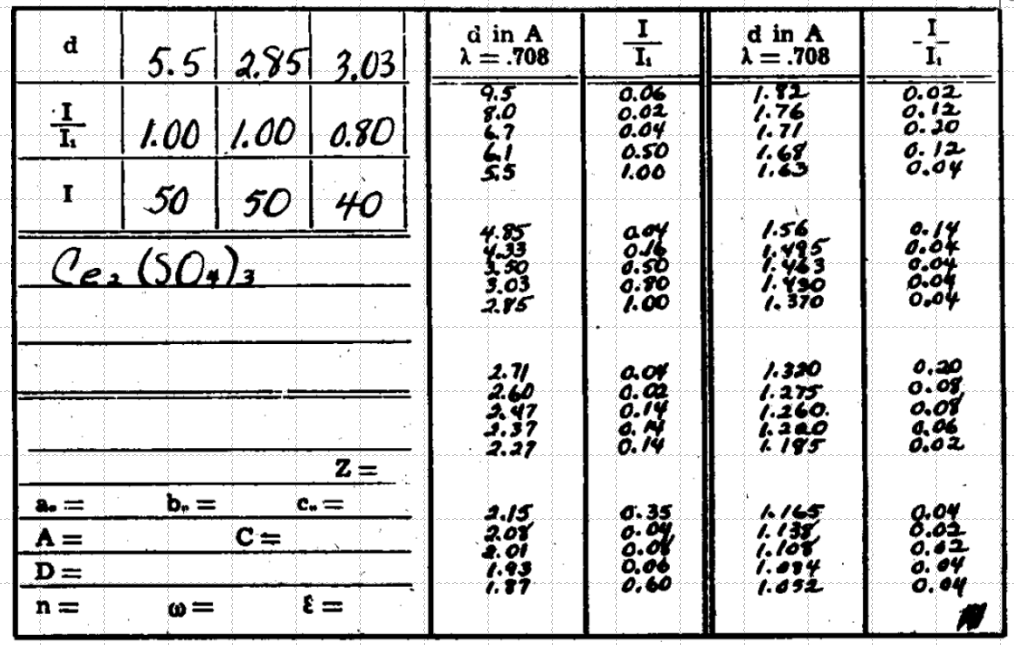

d	5.5	2.85	3.03
$\frac{I}{I_1}$	1.00	1.00	0.80
I	50	50	40

$Ce_2(SO_4)_3$

Z =

a_o = b_o = c_o =

A = C =

D =

n = ω = ε =

d in A λ = .708	$\frac{I}{I_1}$	d in A λ = .708	$\frac{I}{I_1}$
9.5	0.06	1.82	0.02
8.0	0.02	1.76	0.12
6.7	0.04	1.71	0.20
6.1	0.50	1.68	0.12
5.5	1.00	1.63	0.04
4.85	0.04	1.56	0.14
4.33	0.16	1.495	0.04
3.50	0.50	1.463	0.04
3.03	0.80	1.430	0.04
2.85	1.00	1.370	0.04
2.71	0.04	1.320	0.20
2.60	0.02	1.275	0.08
2.47	0.14	1.260	0.08
2.37	0.14	1.220	0.06
2.27	0.14	1.185	0.02
2.15	0.35	1.165	0.04
2.08	0.04	1.138	0.02
2.01	0.08	1.108	0.02
1.93	0.06	1.094	0.04
1.87	0.60	1.052	0.04

Card image for $Ce_2(SO_4)_3$ from PDF Set 1 as issued in 1941

Source: ICDD

Powder Diffraction File (PDF) Database

- 1962, the d-I's, formulas, and PDF numbers were first keyboarded for a computer-readable database.
- 1969 -- the Joint Committee on Powder Diffraction Standards (JCPDS) was formed as a non-profit corporation to oversee the database
- By 1971 the Powder Diffraction File (PDF) contained 21 sets of data with about 21,500 entries
- 1978 – name change to the International Centre for Diffraction Data (ICDD)
- PDF-4 Release 2011
  - 316,291 total datasets

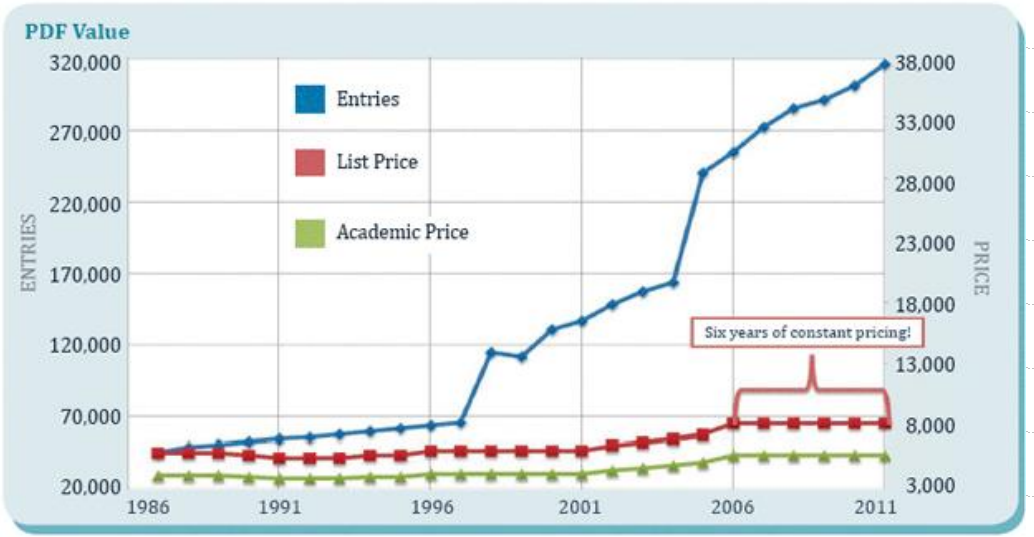

ICDD® International Centre for Diffraction Data

Source: ICDD

Computer Searching of the PDF

- Computerization has dramatically improved the efficiency of searching the JCPDS database
- Cards are no longer printed – data are on CD-ROM
- Numerous third-party vendors have software for searching the PDF database
- Computerized "cards" can contain much more crystallographic information
- Evolution of the database is continuing…

Experimental Issues and Problems

- Searching of the PDF requires high-quality data
  - ***accurate*** line positions are a must!
  - calibration of camera and diffractometer with known *d* - spacing standards
  - careful measurement of line intensities
  - elimination of artifacts (e.g. preferred orientation)
  - solid solutions and strains shift peak positions
- "garbage in, garbage out" -- poor quality data will usually give a poor match
- mixtures of two or more phases
- errors in the database

Whole Pattern Fitting

- Traditional quantitative phase analysis focuses on the intensities of one or a small number of peaks
- Greater accuracy can be obtained by fitting the whole diffraction pattern to what would be expected for a mixture of components
- This approach gives an analysis that is an average over all of the peaks, so it is less susceptible to errors that arise from preferred orientation or poor particle statistics
- The Rietveld method fits the whole of the diffraction pattern to calculated intensities for the various phases that are present. Gives crystal structure information as well as composition.

XRD on Mars

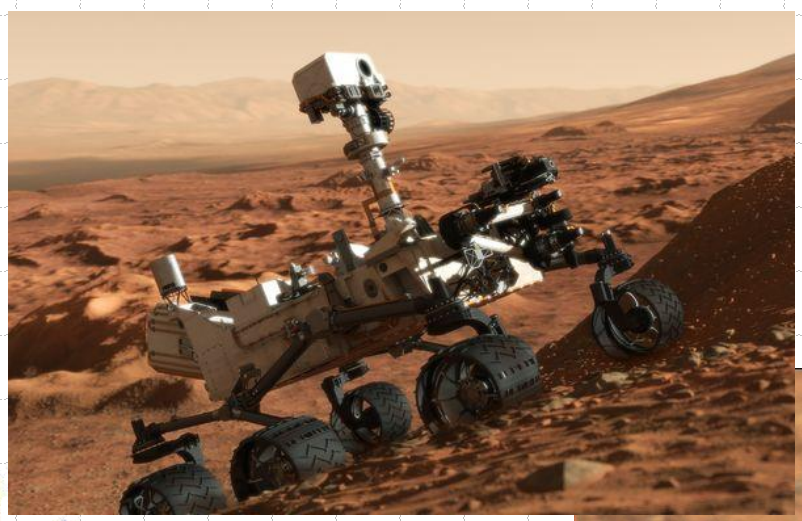

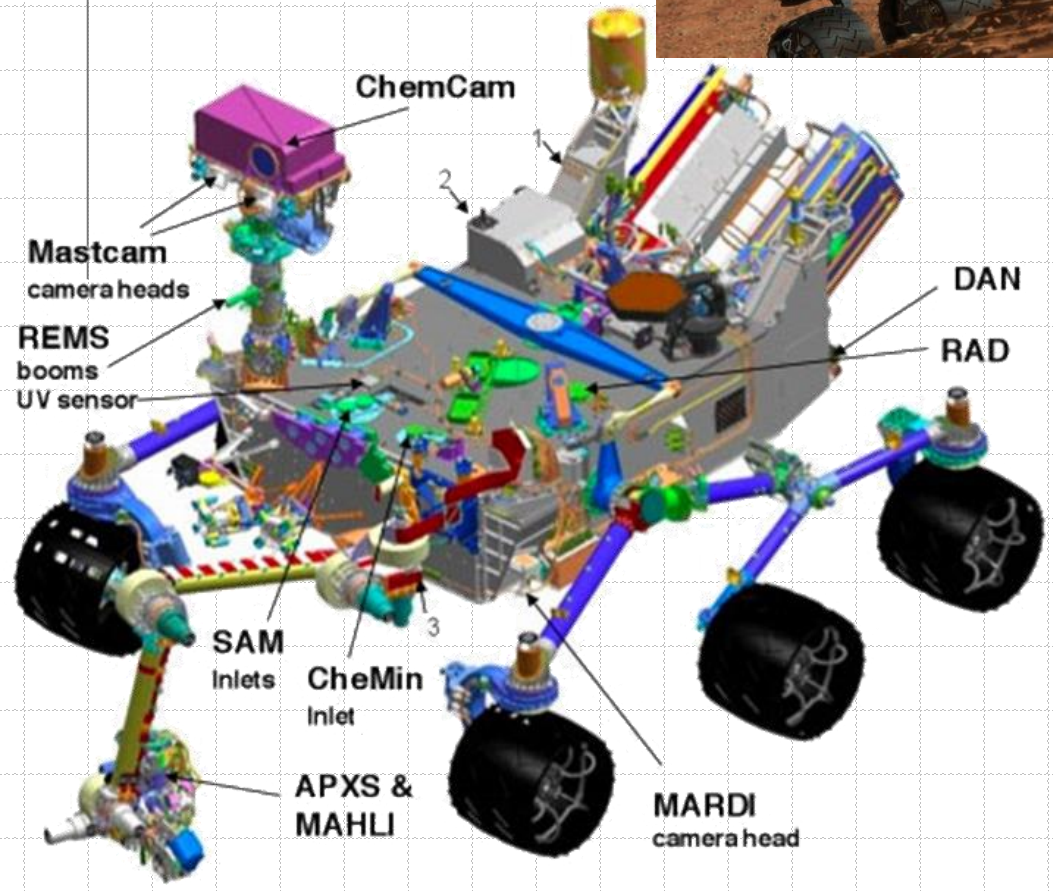

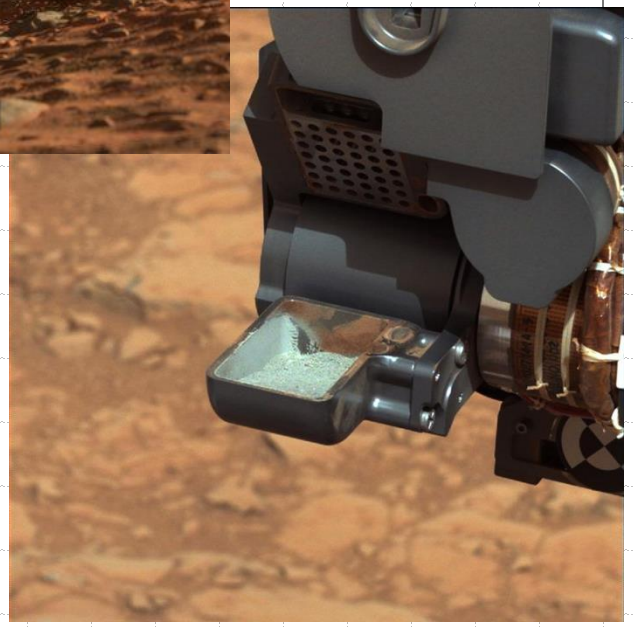

This image from NASA's Curiosity rover shows the first sample of powdered rock extracted by the rover's drill. The image was taken after the sample was transferred from the drill to the rover's scoop. In planned subsequent steps, the sample will be sieved, and portions of it delivered to the Chemistry and Mineralogy instrument and the Sample Analysis at Mars instrument.

XRD on Mars

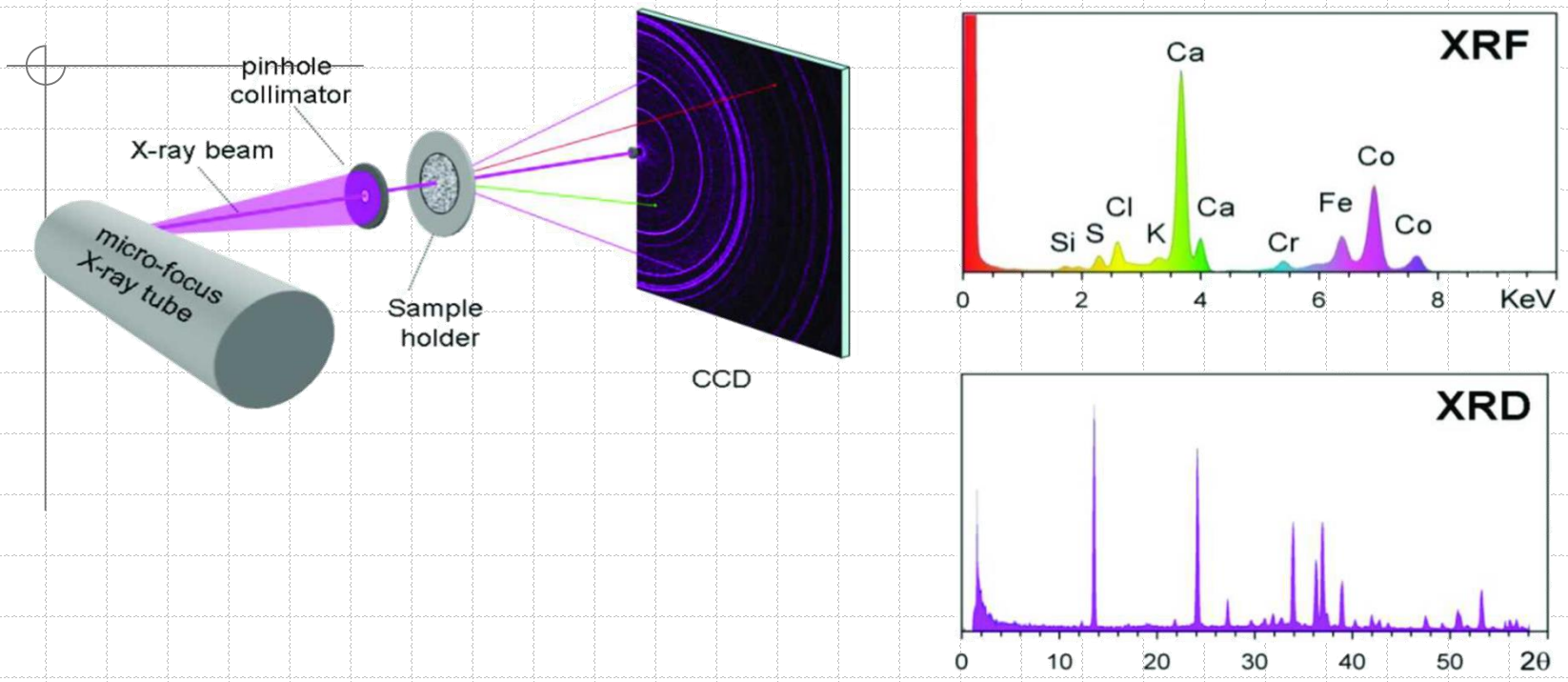

Schematic diagram of the CheMin instrument and resulting XRF and XRD data.

XRD on Mars

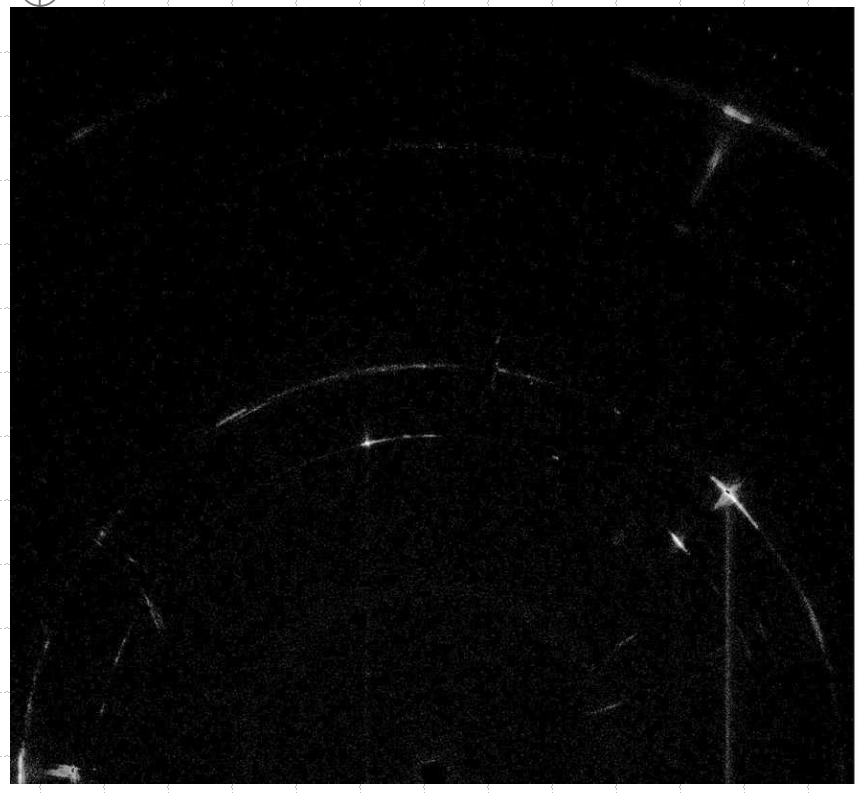

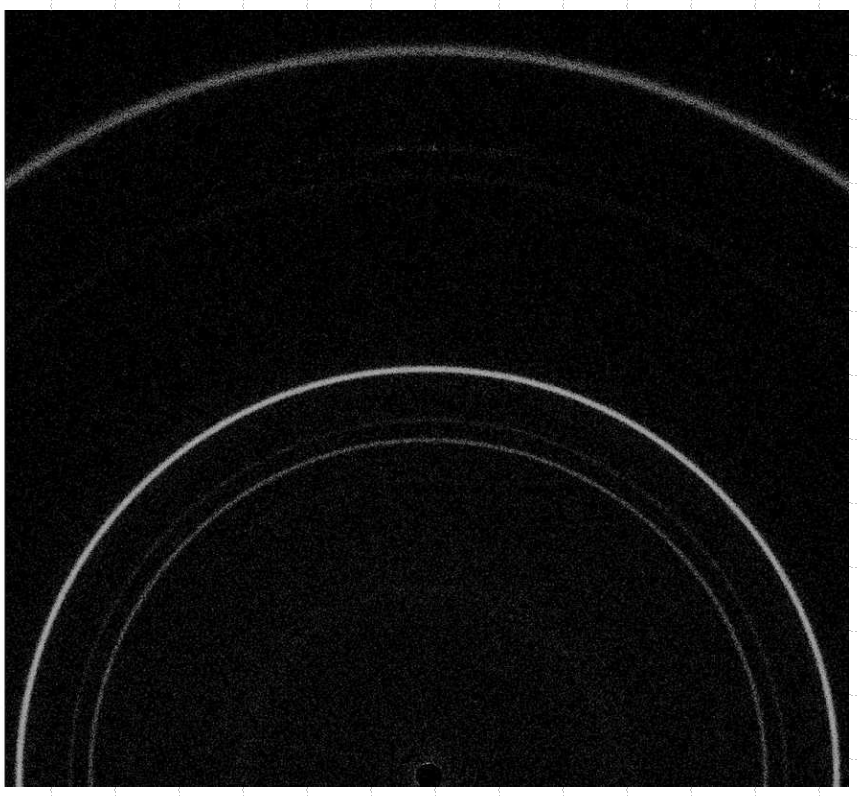

XRD patterns of crushed and sieved (150 μm) NaCl measured on the CheMin III instrument, (left) without and (right) with sonic vibration.

XRD on Mars

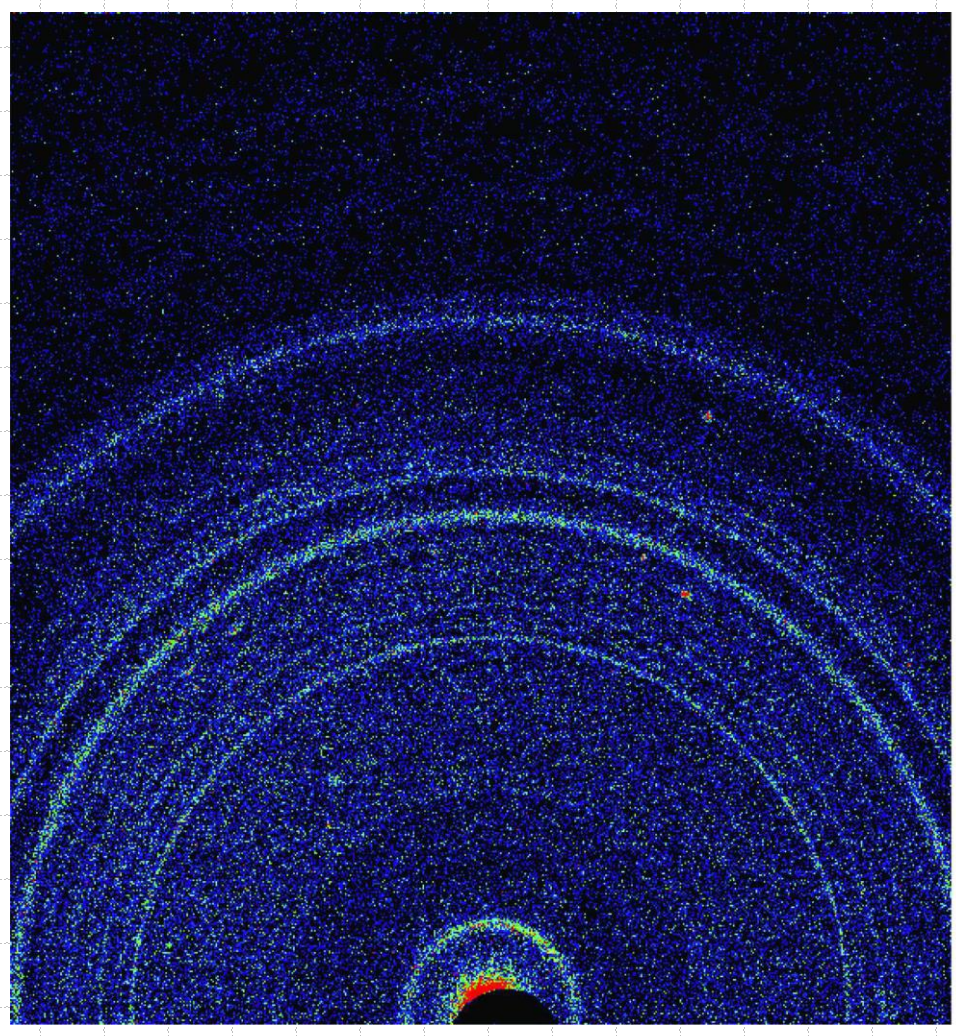

A two-dimensional XRD pattern for the Rocknest aeolian bedform (dune).

Bish *et al.*
IUCrJ **Volume 1** | **Part 6** | November 2014 | Pages 514–522 | 10.1107/S2052252514021150

XRD on Mars

Mineral	Weight (%)
Plagioclase	30
Forsterite-Fe	16
Augite	11
Pigeonite	10
Magnetite	1.5
Anhydrite	1.1
Quartz	1.0
Sanidine†	1.0
Hematite†	0.8
Ilmenite†	0.9
Amorphous	27

†At or near the detection limit.

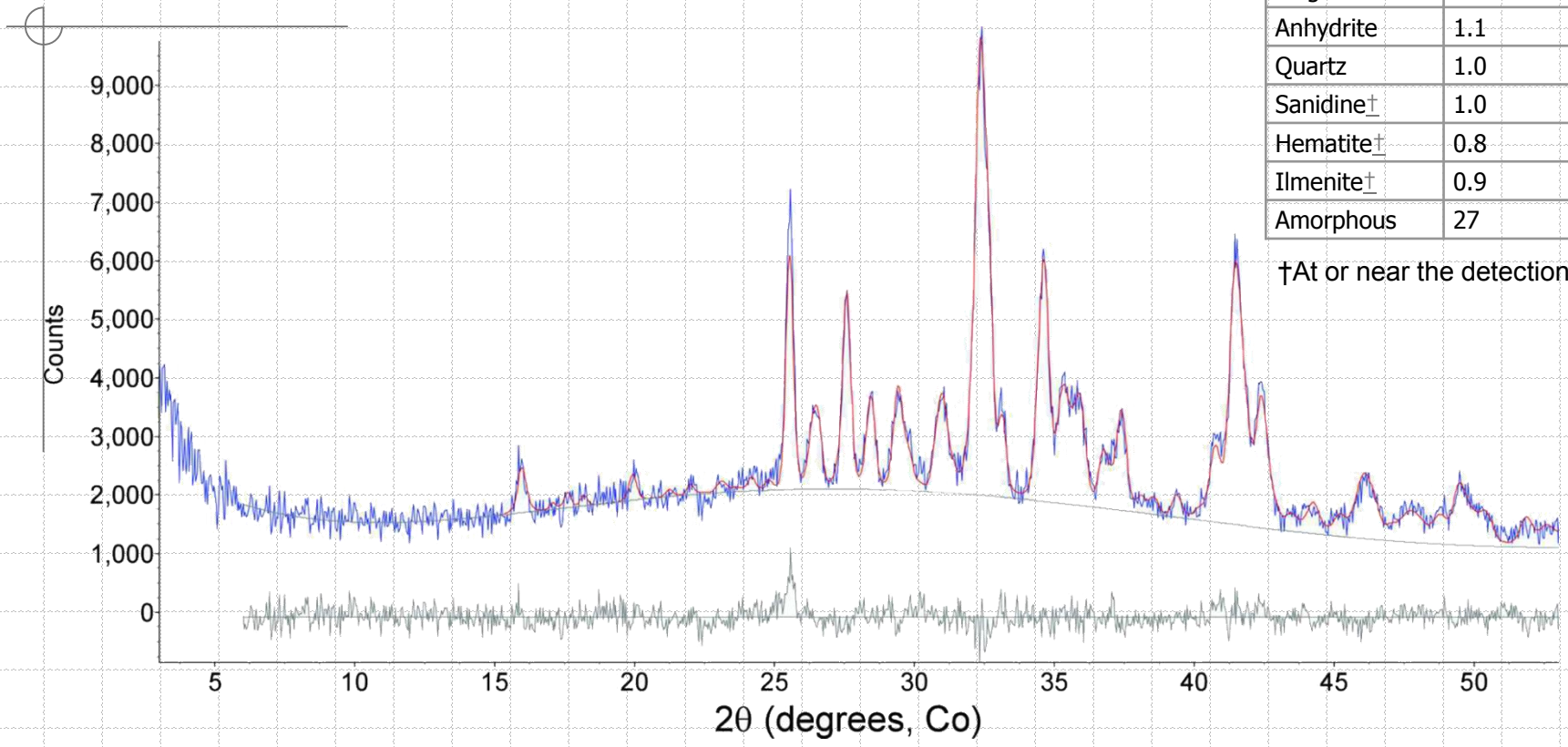

Observed (blue, integrated from the two-dimensional image in Fig.6) and calculated (red) plots from Rietveld refinement using data for Rocknest (~26.4 h integration, phases listed in Table1).

Whole Pattern Fitting - Example: $LiFePO_4$

Excellent candidate for the cathode of rechargeable lithium battery that is inexpensive, nontoxic, and environmentally benign.

First Reported:

"$LiFePO_4$: A Novel Cathode Material for Rechargeable Batteries",
A.K. Padhi, K.S. Nanjundaswamy, J.B. Goodenough, Electrochimical Society Meeting Abstracts, **96-1**, May, 1996, pp 73.

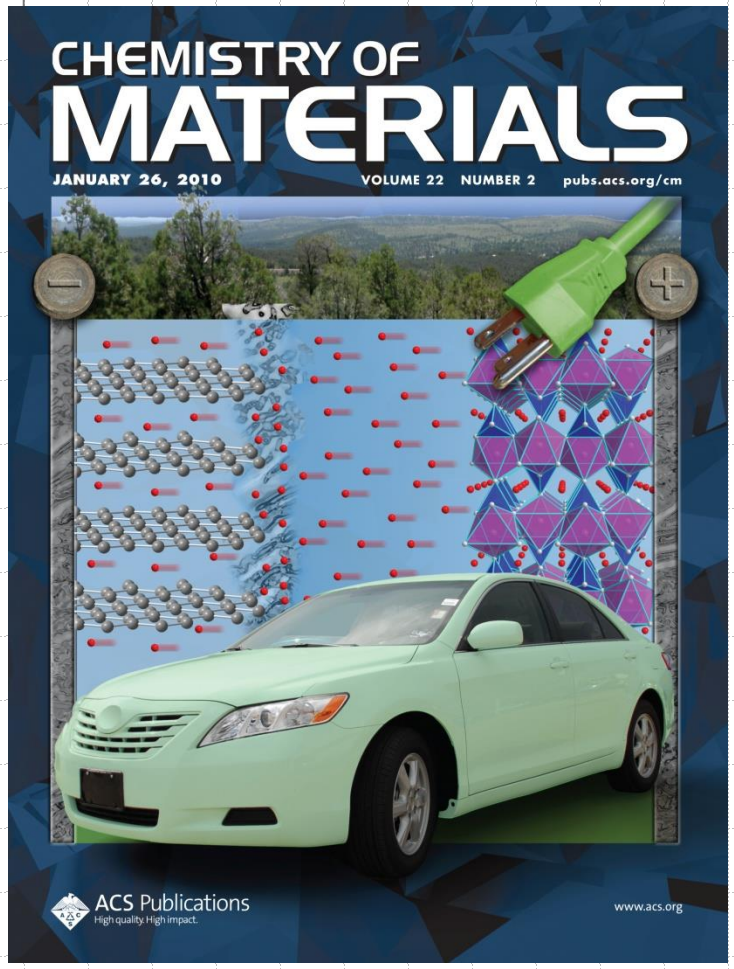

Structure of $LiFePO_4$

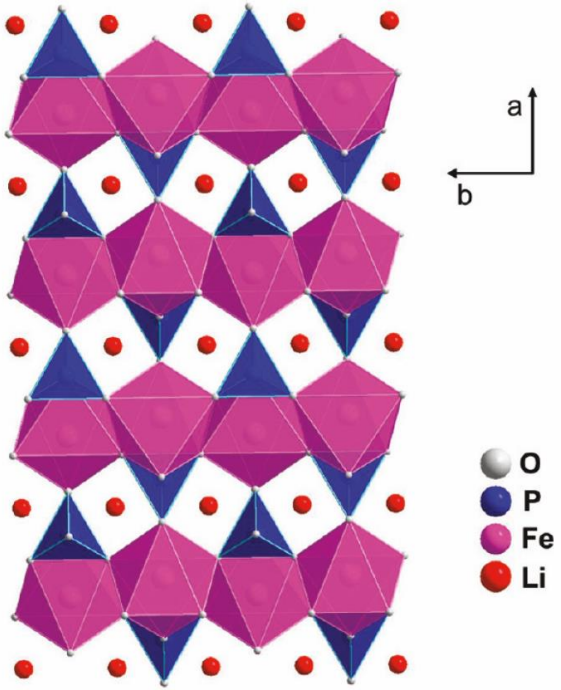

Padhi, A. K.; Nanjundaswamy, K. S.; Goodenough, J. B. J. Electrochem. Soc. 1997, 144, 1188

Whole Pattern Fitting - Example: $LiFePO_4$

•When a lithium-based cell is discharging, the lithium is extracted from the anode and inserted into the cathode.
•When the cell is charging, the reverse occurs.

Cathode (Li_xCoO_2: $0 < x < 1$)
Anode (Li_xC_6: $0 < x < 1$)

Commercialized by Sony Corp. in 1991

Limits for the large scale applications:
1. Safety
2. Cost (Co)

Whole Pattern Fitting - Example: $LiFePO_4$

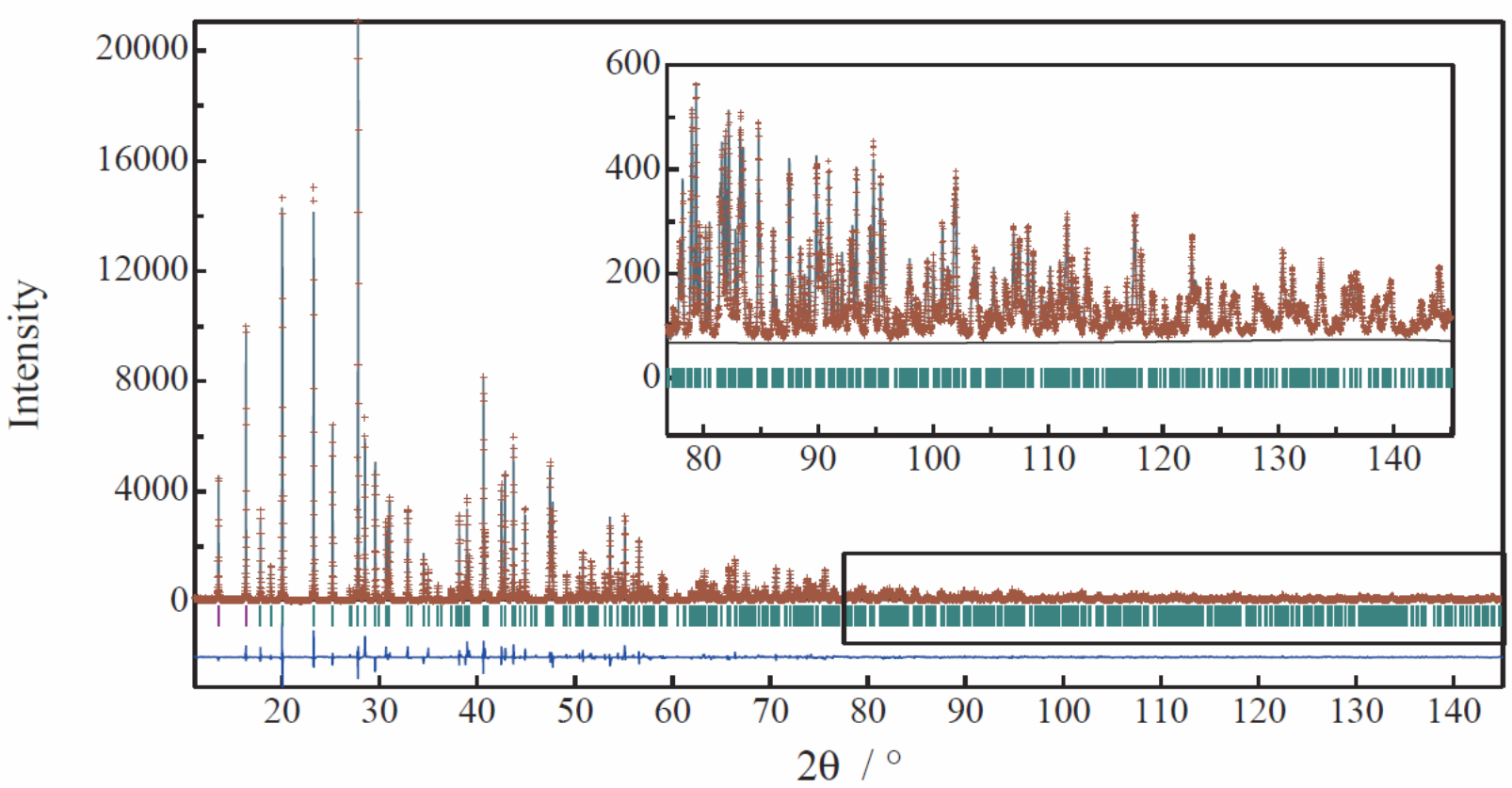

Maximum entropy method (MEM)-based whole-pattern fitting of room temperature high-resolution synchrotron X-ray diffraction data for $LiFePO_4$. The incident beam from the bending magnet source was monochromated by a double-crystal Si (111) monochromator, and the diffraction data were collected by a multiple-detector system with flat Ge (111) analysis crystals and scintillation counters. The wavelength was calibrated as 1.206353 Å by powder diffraction data from NIST SRM640c.

Whole Pattern Fitting - Example: $LiFePO_4$

"Experimental visualization of lithium diffusion in Li_xFePO_4"
Shin-ichi Nishimura, Genki Kobayashi, Kenji Ohoyama, Ryoji Kanno, Masatomo Yashima & Atsuo Yamada
Nature Materials **7**, 707 (2008) Published online: 10 August 2008

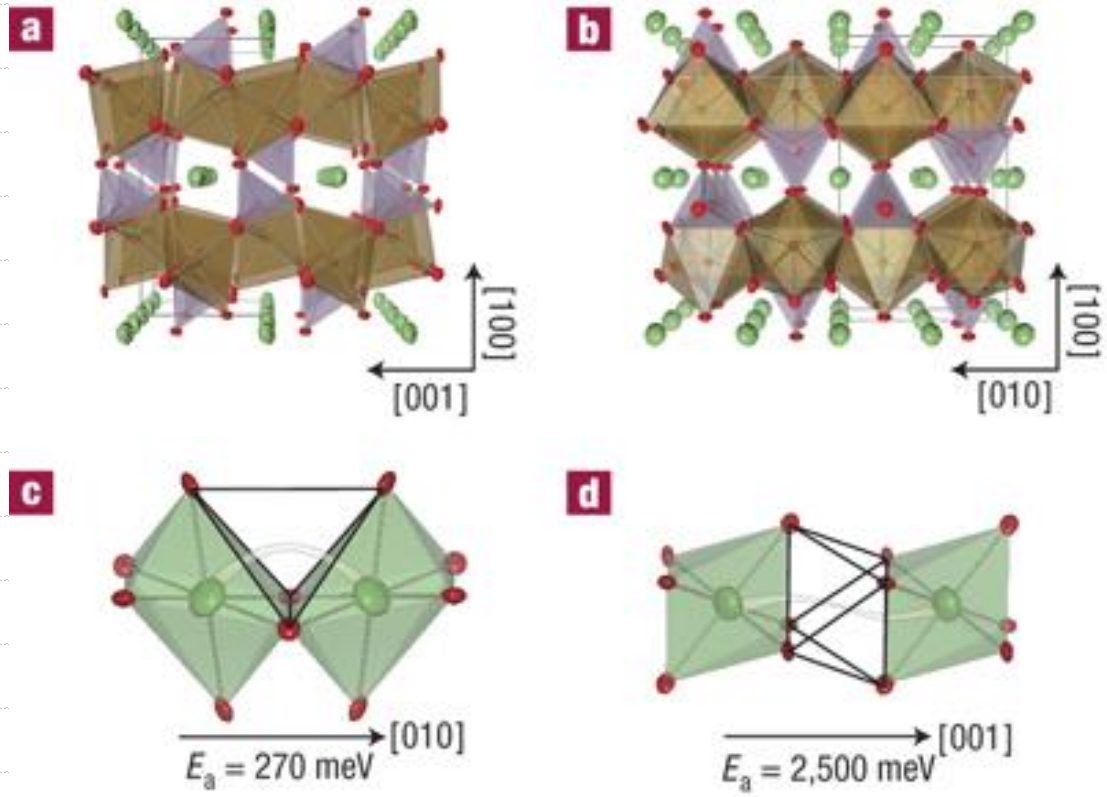

Whole Pattern Fitting - Example: $LiFePO_4$

a

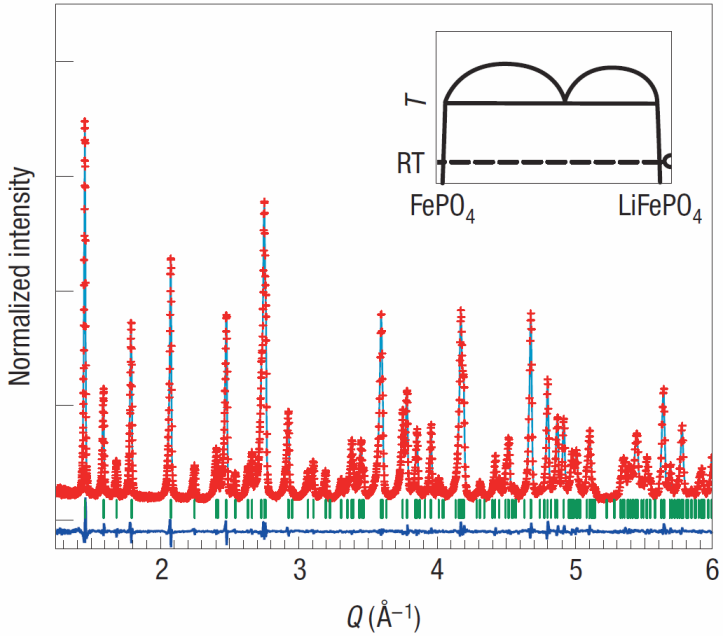

Atom	Wyckoff	g	x	y	z
Li	4a	1	0	0	0
Fe	4c	1	0.28210(6)	1/4	0.97535(19)
P	4c	1	0.09512(12)	1/4	0.4180(3)
O (1)	4c	1	0.09709(12)	1/4	0.7418(3)
O (2)	4c	1	0.45693(11)	1/4	0.2060(3)
O (3)	8d	1	0.15474(9)	0.04636(14)	0.28508(16)

Atom	U_{11} / Å^2	U_{22} / Å^2	U_{33} / Å^2	U_{12} / Å^2	U_{13} / Å^2	U_{23} / Å^2	B_{eq}
Li	0.022(2)	0.0190(18)	0.0156(19)	-0.0027(15)	-0.002(2)	-0.0053(19)	1.51
Fe	0.0043(4)	0.0045(4)	0.0062(4)	0	0.0003(3)	0	0.40
P	0.0036(6)	0.0036(6)	0.0035(7)	0	0.0007(6)	0	0.28
O (1)	0.0084(6)	0.0075(7)	0.0029(7)	0	-0.0005(5)	0	0.49
O (2)	0.0038(7)	0.0080(6)	0.0065(7)	0	0.0003(5)	0	0.48
O (3)	0.0085(5)	0.0048(4)	0.0064(5)	0.0034(4)	0.0011(4)	-0.0005(4)	0.52

$a = 10.32884(19)$ Å, $b = 6.00684$ Å, $c = 4.69236(8)$ Å, $V = 291.131(9)$ Å^3

$R_{wp} = 2.66\%$, $R_p = 2.17\%$, $S = 1.34$, $R_I = 0.46\%$, $R_F = 0.47\%$

Rietveld refinement results for $LiFePO_4$ with neutron diffraction data measured at room temperature in air.

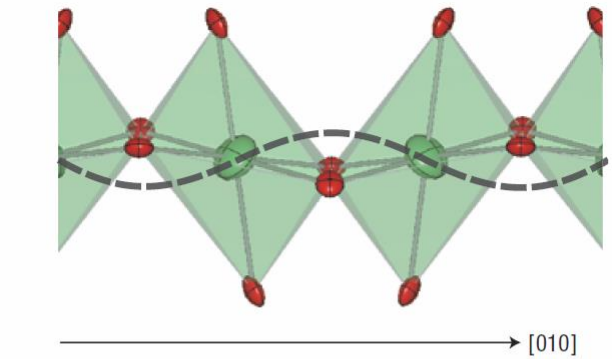

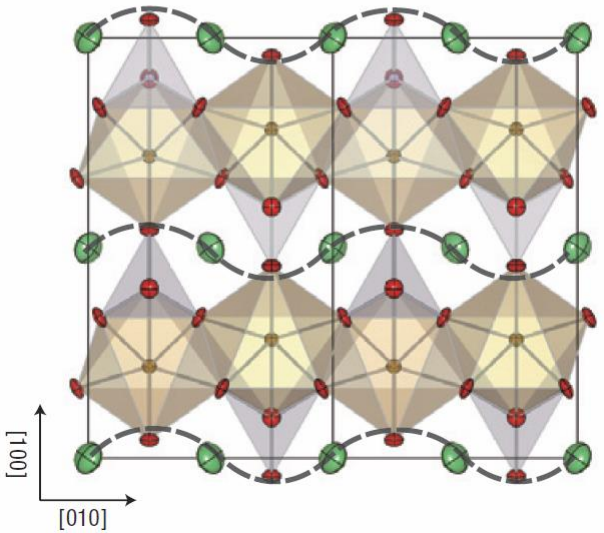

Whole Pattern Fitting - Example: $LiFePO_4$

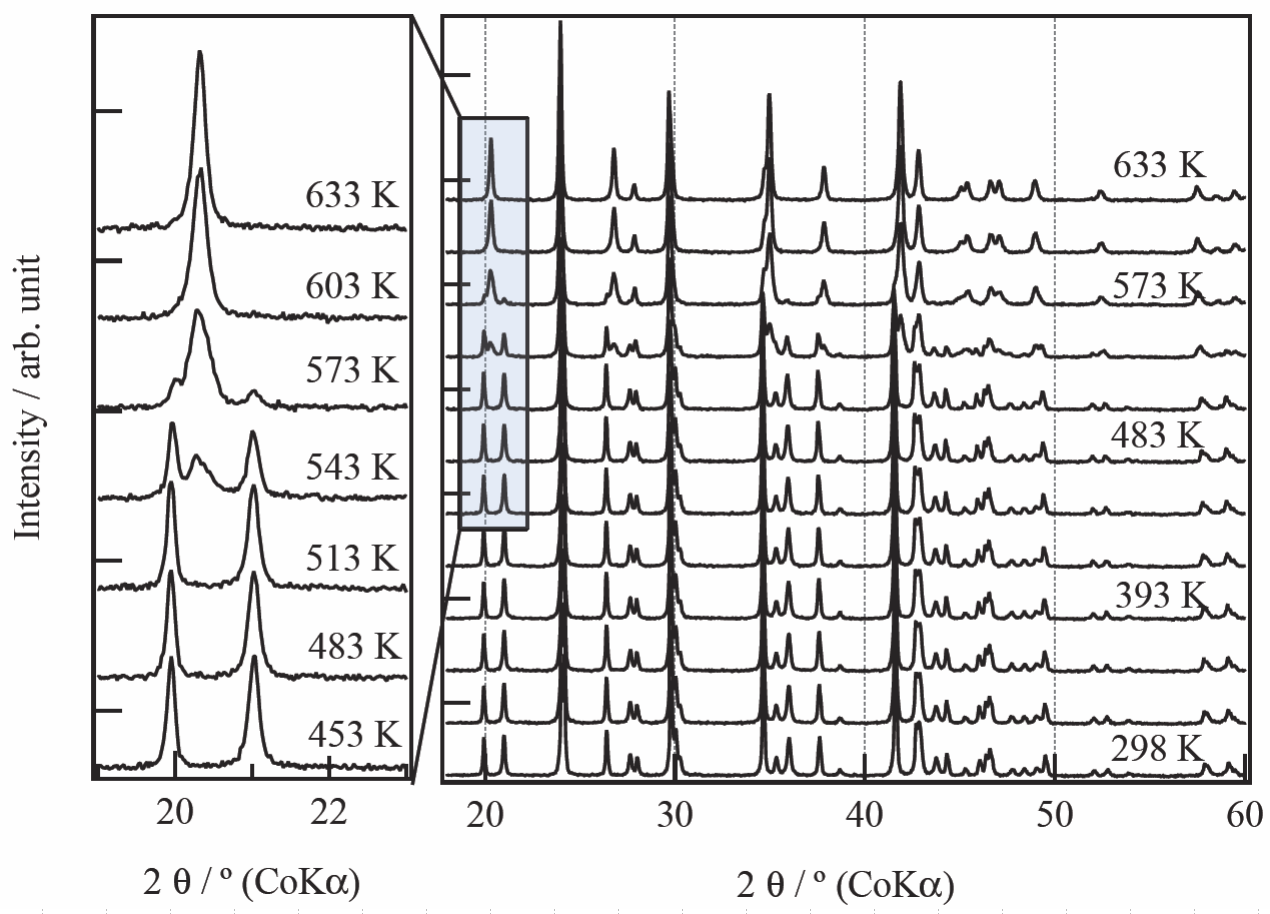

X-ray diffraction patterns of a mixture of 0.6 $LiFePO_4$ and 0.4 $FePO_4$ recorded at 30 K steps from 298 K to 633 K with magnification of 200 reflections. Bruker AXS D8 ADVANCE powder diffractometer was used with Co-Kα radiation and linear position-sensitive detector Vantec-1. Measurement ranges were from 15° to 100°. The measurements were conducted under a high-purity He atmosphere in an Anton Paar HTK 450 temperature-controlled chamber.

Whole Pattern Fitting - Example: $LiFePO_4$

a

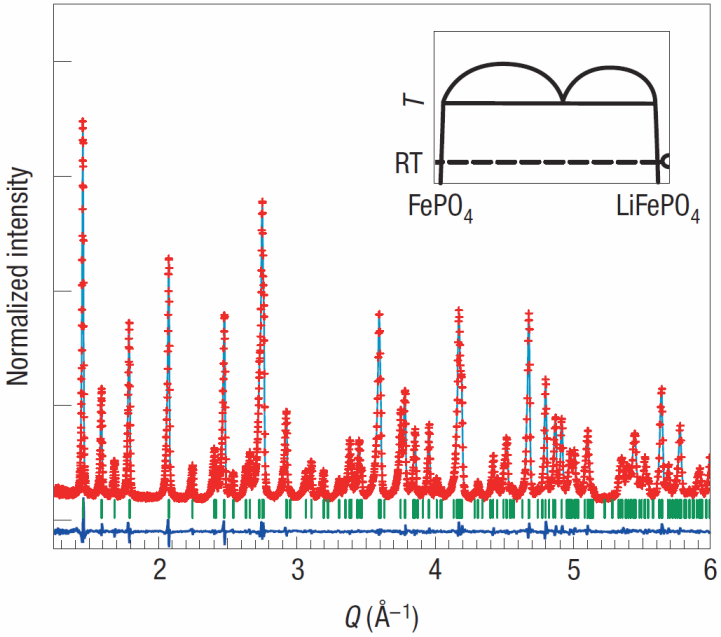

Atom	Wyckoff	g	x	y	z
Li	4a	1	0	0	0
Fe	4c	1	0.28210(6)	1/4	0.97535(19)
P	4c	1	0.09512(12)	1/4	0.4180(3)
O (1)	4c	1	0.09709(12)	1/4	0.7418(3)
O (2)	4c	1	0.45693(11)	1/4	0.2060(3)
O (3)	8d	1	0.15474(9)	0.04636(14)	0.28508(16)

Atom	U_{11} / Å^2	U_{22} / Å^2	U_{33} / Å^2	U_{12} / Å^2	U_{13} / Å^2	U_{23} / Å^2	B_{eq}
Li	0.022(2)	0.0190(18)	0.0156(19)	-0.0027(15)	-0.002(2)	-0.0053(19)	1.51
Fe	0.0043(4)	0.0045(4)	0.0062(4)	0	0.0003(3)	0	0.40
P	0.0036(6)	0.0036(6)	0.0035(7)	0	0.0007(6)	0	0.28
O (1)	0.0084(6)	0.0075(7)	0.0029(7)	0	-0.0005(5)	0	0.49
O (2)	0.0038(7)	0.0080(6)	0.0065(7)	0	0.0003(5)	0	0.48
O (3)	0.0085(5)	0.0048(4)	0.0064(5)	0.0034(4)	0.0011(4)	-0.0005(4)	0.52

$a = 10.32884(19)$ Å, $b = 6.00684$ Å, $c = 4.69236(8)$ Å, $V = 291.131(9)$ Å^3

$R_{wp} = 2.66\%$, $R_p = 2.17\%$, $S = 1.34$, $R_I = 0.46\%$, $R_F = 0.47\%$

Rietveld refinement results for $LiFePO_4$ with neutron diffraction data measured at room temperature in air.

b

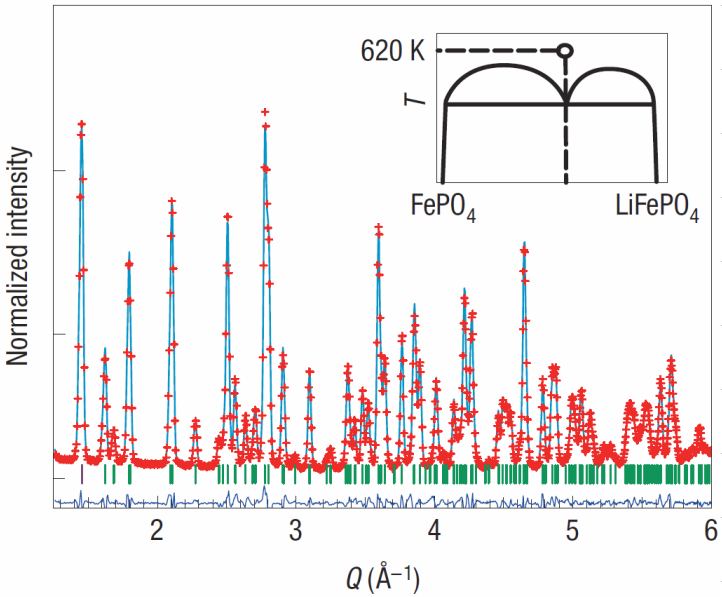

Atom	Wyckoff	g	x	y	z	B_{iso} /Å^2
Li	4a	0.6	0	0	0	3.4(3)
Fe	4c	1	0.28059(13)	1/4	0.9706(3)	-
P	4c	1	0.0954(3)	1/4	0.4184(5)	-
O (1)	4c	1	-0.8898(3)	1/4	0.7343(4)	-
O (2)	4c	1	0.4542(3)	1/4	0.1806(5)	-
O (3)	8d	1	0.16810(18)	0.0477(3)	0.2792(4)	-

Atom	U_{11} / Å^2	U_{22} / Å^2	U_{33} / Å^2	U_{12} / Å^2	U_{13} / Å^2	U_{23} / Å^2	B_{eq}
Li	–	–	–	–	–	–	–
Fe	0.0150(9)	0.0119(8)	0.0133(9)	0	-0.0010(7)	0	1.06
P	0.0173(18)	0.0164(14)	0.0060(15)	0	0.0005(13)	0	1.04
O (1)	0.0271(18)	0.0256(15)	0.074(15)	0	-0.0018(15)	0	1.58
O (2)	0.0176(17)	0.0262(16)	0.0131(16)	0	0.0050(10)	0	1.50
O (3)	0.0181(11)	0.0187(8)	0.0211(11)	0.0018(9)	0.0059(9)	-0.0071(10)	1.53

$a = 10.1763(9)$ Å, $b = 5.9683(5)$ Å, $c = 4.7733(4)$ Å, $V = 289.91(4)$Å^3

$R_{wp} = 3.65\%$, $R_p = 2.75\%$, $S = 3.37$, $R_I = 0.66\%$, $R_F = 0.32\%$

Rietveld refinement results for $Li0.6FePO_4$ using neutron diffraction data measured at 620 K in Ar.

Whole Pattern Fitting - Example: $LiFePO_4$

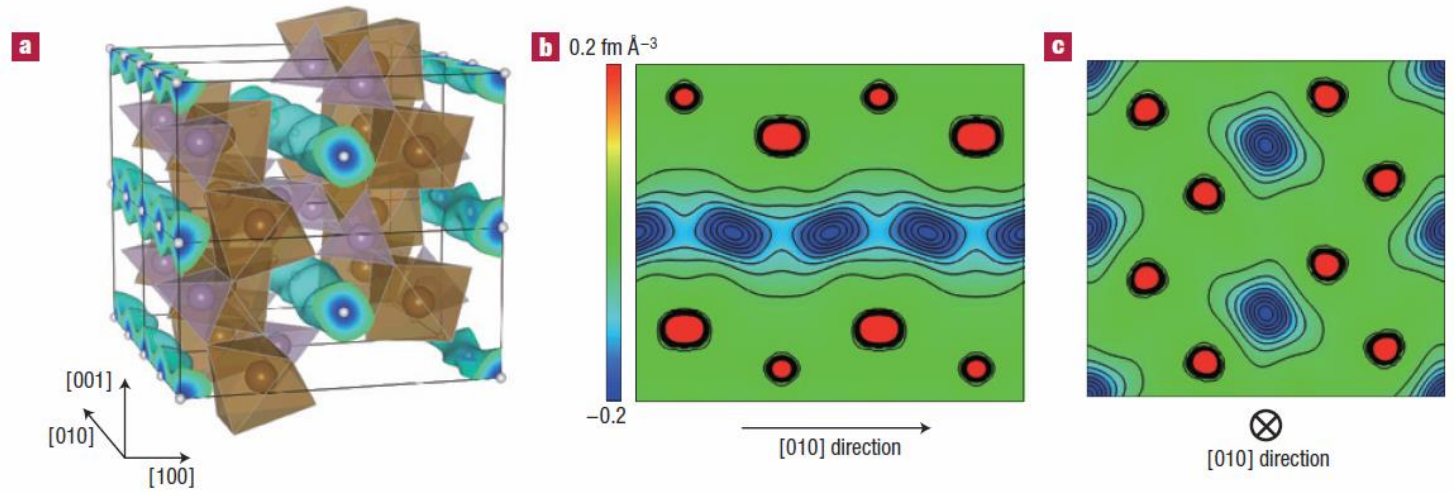

Nuclear distribution of lithium calculated by the Maximum Entropy Method (MEM) using neutron powder diffraction data measured for $Li_{0.6}FePO_4$ at 620 K.

(a) Three-dimensional Li nuclear density data shown as blue contours. The brown octahedra represent FeO_6 and the purple tetrahedra represent PO_4 units.

(b) Two-dimensional contour map sliced on the (001) plane at z = 0.5; lithium delocalizes along the curved one-dimensional chain along the [010] direction, whereas Fe, P and O remain near their original positions.

(c) Two-dimensional contour map sliced on the (010) plane at y = 0; all atoms remain near their original positions.